catalysts

MDPI

Article

Deactivation and Regeneration of Palladium Catalysts for Hydrogenation Debenzylation of 2,4,6,8,10,12-Hexabenzyl -2,4,6,8,10,12-Hexaazaisowurtzitane (HBIW)

Qunfeng Zhang *, Mei Wang, Jiacheng Qian, Shuyuan Lou, Jianhong Jin, Bingcheng Li, Chunshan Lu, Feng Feng, Jinghui Lv, Qingtao Wang * and Xiaonian Li *

State Key Laboratory Breeding Base of Green Chemistry Synthesis Technology,
Institute of Industrial Catalysis of Zhejiang, University of Technology, Hangzhou 310014, China
* Correspondence: zhangqf@zjut.edu.cn (Q.Z.); qtwang@zjut.edu.cn (Q.W.); xnli@zjut.edu.cn (X.L.)

Abstract: 2,4,6,8,10,12-hexanitro-2,4,6,8,10,12-hexaazaisowurtzitane (HNIW, also known as CL-20) is an important energetic compound. As one of the representatives of the third generation of energetic materials, it has an excellent performance, providing broad application prospects for the development of new weapons and equipment. The synthesis of CL-20 is usually obtained from 2,4,6,8,10,12-hexabenzyl-2,4,6,8,10,12-hexaazaisowurtzitane (HBIW) through two catalytic hydrogenolysis and debenzylation reactions, followed by nitration. The most critical step is the hydrogenolysis debenzyl-acetylation process of HBIW because this process requires a large amount of expensive palladium-based catalyst, and the catalyst is completely deactivated after one use. In response to this problem, there is no suitable solution at present, resulting in the high cost of the entire synthesis process. Therefore, reducing the production cost of CL-20 by increasing the catalyst stability is one of the current research priorities. By using AAS, XRD, XPS, TEM, BET, TG and other characterization techniques, the reasons for catalyst deactivation were explored. Studies have shown that the main reason for catalyst deactivation is that a large number of blockages accumulate in the pores of the catalyst after the reaction, which greatly weakens the transfer of the reactant HBIW, intermediate substances, and product 2,6,8,12-tetraacetyl-4,10-dibenzyl-2,4,6,8,10,12-hexaazaisowurtzitane (TADBIW) in the catalyst pores, and the blockage may block the active site of the catalyst. A regeneration treatment method for catalyst deactivation was developed. This method uses chloroform and glacial acetic acid as reagents, which, when combined with stirring and ultrasonic operation, finally restores the activity of the $Pd(OH)_2/C$ catalyst. The BET and TG parameters of the regenerated catalyst indicate that catalyst textural and structural properties have greatly recovered, indicating that this treatment method can remove the blockages in the catalyst pores.

Keywords: HBIW; TADBIW; $Pd(OH)_2/C$ catalyst; inactivation and regeneration; hydrodebenzylation

Citation: Zhang, Q.; Wang, M.; Qian, J.; Lou, S.; Jin, J.; Li, B.; Lu, C.; Feng, F.; Lv, J.; Wang, Q.; et al. Deactivation and Regeneration of Palladium Catalysts for Hydrogenation Debenzylation of 2,4,6,8,10,12-Hexabenzyl-2,4,6,8,10,12-Hexaazaisowurtzitane (HBIW). *Catalysts* **2022**, *12*, 1547. https://doi.org/10.3390/catal12121547

Academic Editors: Ning Rui and Lili Lin

Received: 22 October 2022
Accepted: 22 November 2022
Published: 1 December 2022

1. Introduction

2,4,6,8,10,12-hexanitro-2,4,6,8,10,12-hexaazaisowurtzitane (HNIW [1–11], also known as CL-20 [12–19], is a high-energy and high-density compound with the highest density and energy level so far. Synthesis of HNIW by a simple and economical process is a research hotspot in the field of high-energy materials. According to literature reports, the synthesis of CL-20 is mainly divided into three steps: Firstly Benzylamine was condensed with glyoxal to form 2,4,6,8,10,12-hexabenzyl-2,4,6,8,10,12-hexaazaisowurtzitane (HBIW); than the HBIW catalyzed hydrogen debenzylation, that is, the partial or full transformation of the six benzyl groups on HBIW into groups that can stabilize the cage structure and are easily replaced by nitro, namely, the transformation of the nitrate substrate. Finally, HNIW was prepared from the debenzylation product of HBIW by nitration (the reaction is shown in Scheme 1 [17–19]). The most critical step is the hydrogenolysis debenzyl-acetylation process of HBIW [20–25]. However, this process requires a large amount of expensive palladium-based catalyst, and

the catalyst is easily deactivated, which largely restricts the application of HNIW. It is clear that the key problems to be solved using this route are the preparation of a high-efficiency palladium catalyst and the realization of the palladium catalyst's continuous stability. The synthesis of HNIW was first reported by Nielsen [26,27] and further studied by scholars. The catalysts used for the conversion of HBIW to TADBIW [28–30] are all effective Pd-based catalysts [29–34]. The currently developed Pd-based catalysts include commercial Pd/C catalysts, mesoporous-supported catalysts (graphene-like carbon nitride support (g-C_3N_4 [35]), disordered mesoporous carbon supports, carbon nanotube supports [6], ion exchange resin supports [30], TiO_2 [36,37] supports, etc.) and bimetallic catalysts [34,35]. Among them, the graphene-like carbon nitride support (g-C_3N_4 [35]) catalyst used in the conversion of HBIW to TADBIW [38,39] has excellent activity and stability and can be recycled three times. In addition, improving the recyclability of the catalyst provides another option to reduce the cost of the hydrodebenzylation process. Maksimowski et al. [40] reported that after the regeneration of the Pd/C through a complex process, the yield was 42%, which was only half of the catalytic yield of fresh catalysts. The low recyclability of the catalyst is mainly due to the poor stability of the catalyst under reaction conditions and catalyst poisoning. Due to the low stability of the catalyst, $Pd(OH)_2/C$ or Pd/TiO_2 catalysts were used for hydrolyzing HBIW, and the palladium content decreased significantly. In addition, HBIW has higher strain energy due to the cage structure of the matrix. In the hydrogenation process, the weak structure of the substrate may produce nitrogen-rich byproducts [37–40], which may block the active site on Pd/C; the impurities are not easy to remove and the catalyst activity is not easy to recover. The disordered mesoporous carbon-supported $Pd(OH)_2$ catalyst reported by Mingxia Zhang [34] et al. was used for the hydrodebenzylation reaction of HBIW, and the yield of TADBIW was 80%. After regeneration by extraction with chloroform solution, it could be recycled twice and the yield remained above 70%. Therefore, it should be noted that the recyclability of palladium-based catalysts to convert HBIW to TADBIW is even more challenging. Herein, we focus on the key step [39] in the synthetic route of CL-20: the hydrodebenzylation of HBIW into TADBIW. First of all, the reasons for the deactivation [41] of the Pd/C and $Pd(OH)_2/C$ catalysts were explored by series characterization. Then, an effective regeneration technology was obtained for Pd/C and $Pd(OH)_2/C$ catalysts, which can also improve the hydrogenolysis activity and stability. The regenerated $Pd(OH)_2/C$ catalyst can then be recycled three times and maintain a high yield (more than 70%), which is better than the best catalyst recovery effect reported so far.

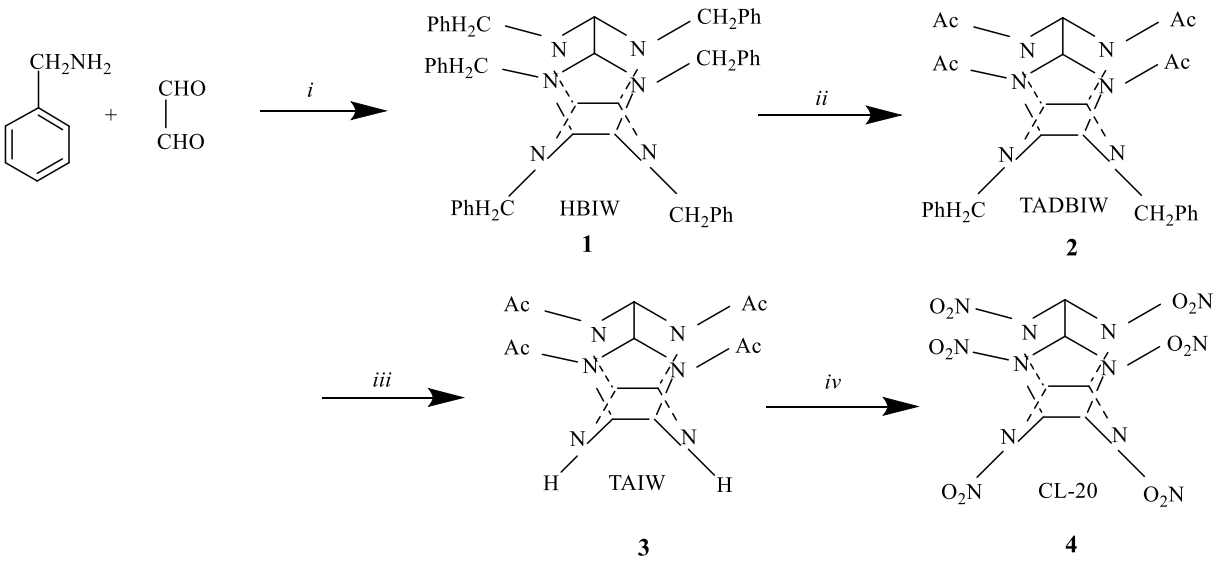

Scheme 1. Synthesis of CL-20.

2. Results and Discussion

The 5 wt.% Pd/C catalysts were treated using the different regeneration methods. The results are shown in Table 1. It can be seen from Table 1 that the most successful catalyst regeneration method used a mixture of chloroform and glacial acetic acid, and the yield of the first application was close to that of fresh 5 wt.% Pd/C. To evaluate the activity of the regenerated catalysts, the hydrogen consumption curve of the initial and secondary application of the catalysts is shown in Figure 1. It is shown that the regenerated Pd/C or Pd $(OH)_2$/C catalysts maintained high activity, indicating that this regeneration treatment method is feasible. For the regenerated 5 wt.% Pd$(OH)_2$/C catalyst, the application test was carried out, and the results are shown in Figure 2. As can be seen from Figure 2, this regeneration method is effective for 5 wt.% Pd$(OH)_2$/C catalyst, and the regenerated catalyst can be recycled for 4 times without a significant decrease in yield.

Table 1. Application of reacted 5 wt.%Pd/C catalyst obtained by different regeneration.

Order Number	Regeneration Treatment Method	TADBIW Yield/%
1	10 wt.% NaOH alkaline solution	0
2	DMF solution (150 °C)	0
3	DMF solution (180 °C)	0
4	DMF solution (200 °C)	0
5	N_2Atmospbaking treatment (250 °C)	0
6	N_2Atmospbaking treatment (300 °C)	0
7	N_2Atmospbaking treatment (350 °C)	0
8	Chloroform and glacial acetic acid mixture treatment	76.29
9	Chloroform and glacial acetic acid mixture treatment	77.84

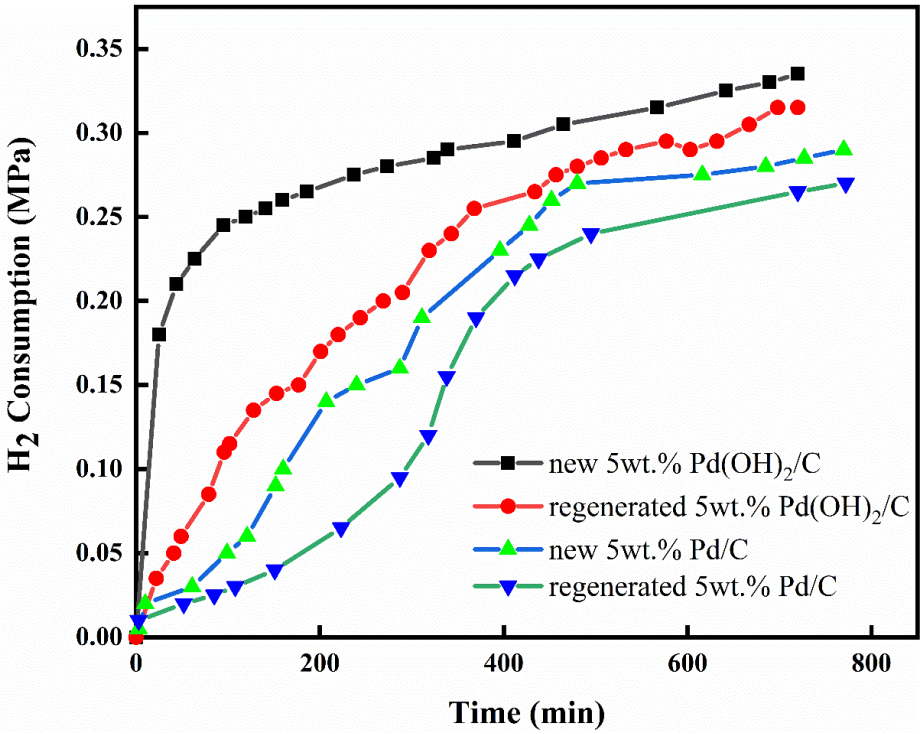

Figure 1. The hydrogen consumption curve for new and regenerated catalysts.

Reaction conditions: 5 g HBIW, 0.5 g regenerated catalyst, 50 mL of DMF, 7 mL of Ac_2O and 0.1 mL of PhBr. The reaction was carried out at 19–20 °C for 4 h, and at 40 °C for another 8 h.

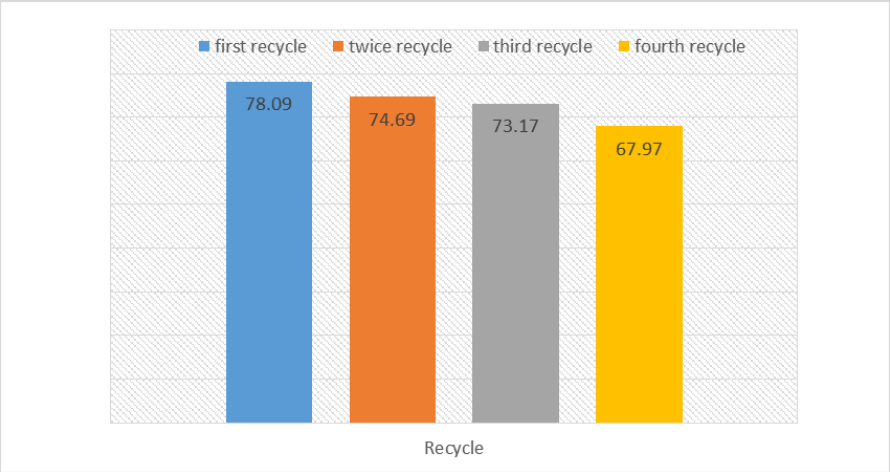

Figure 2. The recycle test results for regenerated 5 wt.% $Pd(OH)_2/C$ catalyst.

As the catalytic activity is affected by the amount of catalyst added, the yield of TADBIW against the different amounts of added catalyst was investigated in detail, and the results are shown in Table 2. It can be seen that the reaction rate can be accelerated by adding more catalyst in a certain range when the substrate is constant. However, excessive use of catalysts can greatly increase the cost. When the content of the catalyst is 10% of HBIW, the achieved yield of TADBIW was 79.71% and with the highest H_2 consumption of 0.300 MPa.

Table 2. Effect of 5 wt.% Pd/C catalyst dosage on TADBIW yield.

Catalyst Amount (x wt% of HBIW)	H_2 Consumption/MPa	Yield/%	Product Melting Point/°C
1	0.035	0	-
2	0.215	0	-
5	0.290	78.01	317~321
10	0.300	79.71	318~322
15	0.300	79.72	316~323

Note: The amount of reactant HBIW was 5 g, 7 mL of Ac_2O, 0.1 mL of PhBr and 50 mL of DMF. The first reaction was at 20 °C for 4 h, and then the temperature was raised to 40 °C for 8 h.

The catalysts before and after the reaction were characterized by TEM. The TEM images of the fresh and spent 5 wt.% Pd/C catalyst are shown in Figure 3a,b, respectively. It can be seen that the Pd was evenly distributed on the carrier before and after the reaction. It was found that the Pd particle size of the fresh 5 wt.% Pd/C catalyst was uniformly distributed in the range of 2–4 nm, with an average particle size of 2.74 nm; the Pd particle size distribution of spent 5 wt.% Pd/C catalyst was mainly in the range of 2 nm~4 nm, with a very small fraction of particles around 5 nm in size and an average particle size of 3.55 nm. The TEM images of fresh and spent 5 wt.% $Pd(OH)_2/C$ catalyst are shown in Figure 3c,d, respectively. The Pd particle size of the 5 wt.% $Pd(OH)_2/C$ catalyst was uniformly distributed in the range of 2 to 5 nm, with an average particle size of 3.30 nm; the Pd particle size of the used 5 wt.% $Pd(OH)_2/C$ catalyst was distributed mainly in the range of 2–4 nm, and the average particle size was 3.48 nm. From the statistical results of particle size, the 5 wt.% $Pd(OH)_2/C$ catalyst particle size of metal Pd before and after the reaction was almost the same. There was no obvious aggregation of the Pd particles after the reaction of the 5 wt.% $Pd(OH)_2/C$ catalyst. Nevertheless, in the spent 5 wt.% Pd/C catalyst (Figure 3b), the palladium particles aggregated and formed large particles, which is one of the reasons for its inactivation.

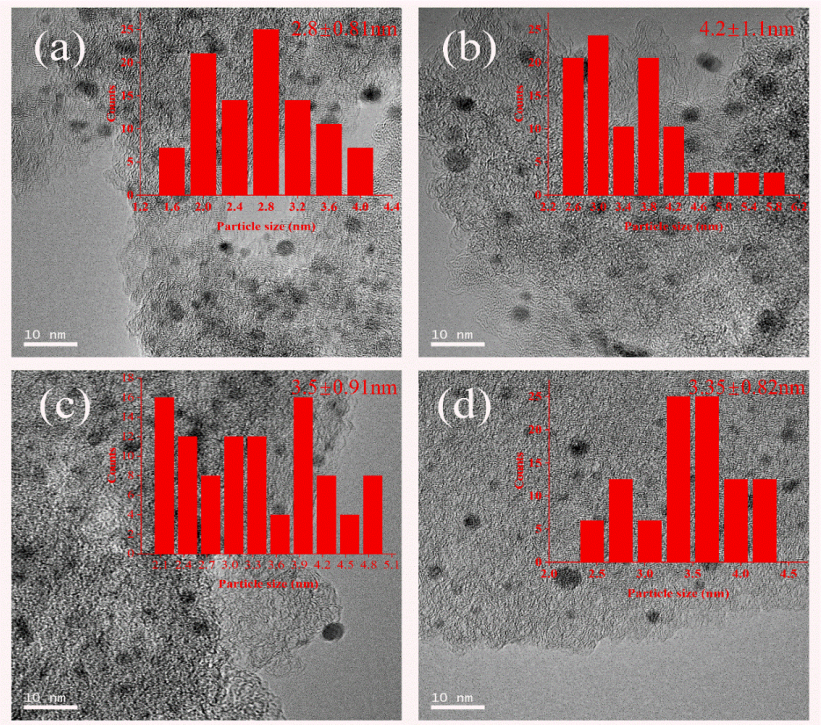

Figure 3. TEM images of fresh and spent catalysts (**a**) fresh 5 wt.% Pd/C catalyst; (**b**) spent 5 wt.% Pd/C (**c**) fresh 5 wt.% $Pd(OH)_2$/C catalyst; and (**d**) spent 5 wt.% $Pd(OH)_2$/C catalyst.

In order to specifically understand the phase structure of the active components of the catalyst, the catalyst samples with 5 wt.% $Pd(OH)_2$/C before and after the reaction were characterized by XRD. As shown in Figure 4, the XRD results show that for the fresh 5 wt.% $Pd(OH)_2$/C catalyst, the diffraction peak at 34.0° is assigned to the PdO (101) crystal plane, the diffraction peak at 42.74° is assigned to the PdO (110) crystal plane, and the 55.02° diffraction peak is assigned to the PdO (112) crystal plane. For the spent 5 wt.% $Pd(OH)_2$/C catalyst, the diffraction peak at 40.03° is attributable to the Pd (111) crystal face, and the diffraction peak at 68.05° is attributable to the Pd (220) crystal plane. After the reaction, the majority of diffraction peaks of PdO disappeared, indicating that the catalyst $Pd(OH)_2$/C had a reduction reaction during the debenzylation action of HBIW. It can be calculated by MDI Jade 6 software that the average grain size of the spent 5 wt.% $Pd(OH)_2$/C catalyst, the particle size was 3.5 nm. Although the average particle size of Pd before and after the reaction catalysts changed, the change range was small, indicating that the Pd particles did not have obvious agglomeration after the reaction.

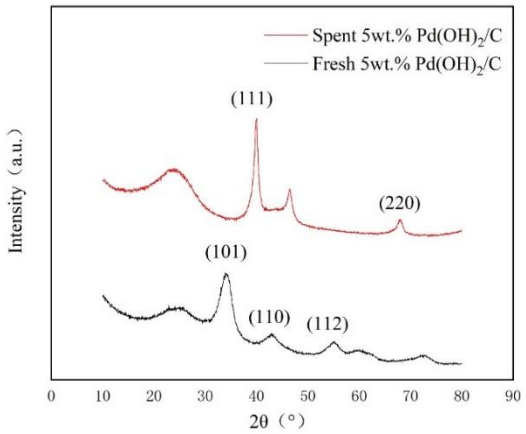

Figure 4. X-ray diffraction patterns of the various catalysts.

Figure 5 shows the XPS spectrum of the Pd 3d lines for the sample before and after the reaction. We can see that the Pd species on the new 5 wt.% $Pd(OH)_2/C$ catalyst all exist in the form of ions. For the spent 5 wt.% $Pd(OH)_2/C$ catalyst, we can see the presence of two palladium states: the ground state (the Pd3d5/2 binding energy is 334.75 eV) corresponds to the metal [11,12] while the other state (the binding energy is 336.25 eV) corresponds to palladium oxide PdO. The atomic ratio of Pd is 0.058 in the spent catalyst. As can be seen, the ratio of the metal Pd increases significantly and there was a decrease in PdO after the reaction.

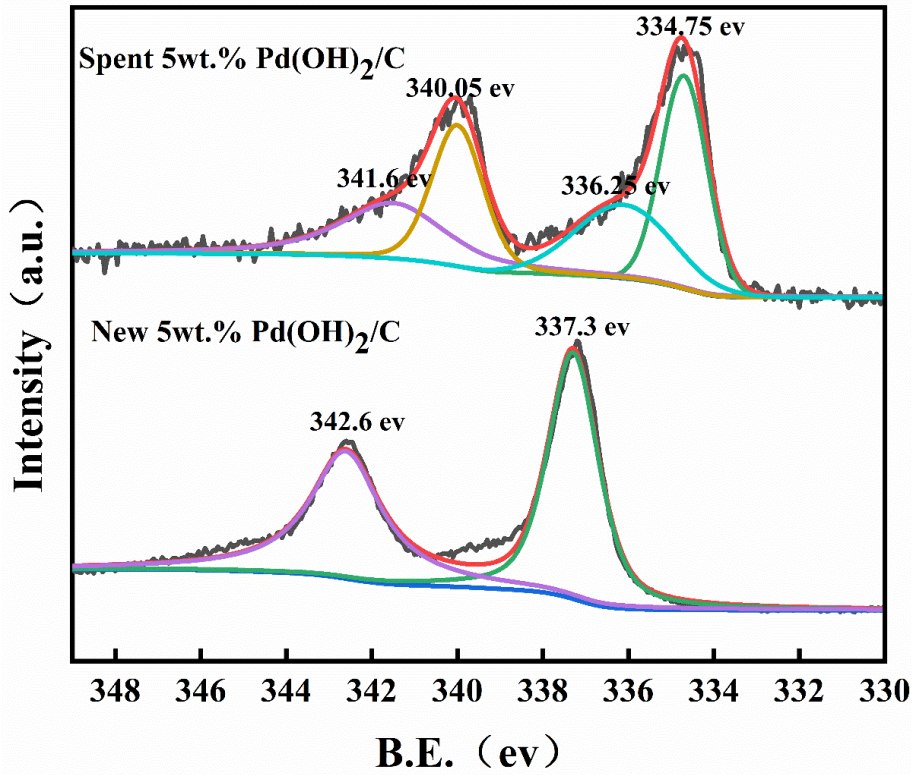

Figure 5. XPS spectrum of Pd 3d lines for the 5 wt.%$Pd(OH)_2/C$ before and after the reaction.

The concentration of Pd in the reaction filtrate was quantitatively analyzed using a TAS-990 atomic absorption spectrometer from China Panalytical Corporation, Beijing, China. The results are shown in Table 3 below. It can be seen from the Table 3 that after the reaction, the content of Pd that had leached into the filtrate was extremely low (<1%), indicating that the loss of metal Pd is not the main factor leading to catalyst deactivation.

Table 3. The AAS results of the reaction filtrate.

Sample	Theoretical Pd Content/mg	Pd Leaching Volume/mg	Pd Extraction Ratio/%
5 wt.% Pd/C	25	0.1741	0.70
5 wt.% $Pd(OH)_2/C$	25	0.1865	0.75

Note: The amount of catalyst added in each reaction is 0.5 g.

In order to study the physical parameters of the catalyst, 5 wt.% of Pd/C and 5 wt.% of $Pd(OH)_2/C$ fresh, spent and regenerated catalysts, respectively, were tested by BET. From the physical adsorption–desorption curves in Figure 6, it can be seen that the adsorption rate increased rapidly at low relative pressures and there was an obvious hysteresis loop of fresh, spent and regenerated 5 wt.% Pd/C and 5 wt.% $Pd(OH)_2/C$ catalyst, which indicated that all samples were dominated by mesopores (close to micropores). It is exactly this property of carbon materials that the supported size of nano Pd particles in its pores is

slightly smaller than the pore size of carbon, which is consistent with the characterization results of TEM. The related parameters are shown in Table 4, and it can be seen that the specific surface area, pore volume and pore size of fresh 5 wt.% Pd/C catalysts were 1493.74 m^2/g, 0.92 cm^3/g and 2.45 nm, respectively, while the spent 5 wt.% Pd/C catalyst only has a specific surface area of 356.38 m^2/g with a pore volume of 0.29 cm^3/g and an average pore size of 3.31 nm. Similarly, the specific surface area, pore volume and pore size of fresh 5 wt.% $Pd(OH)_2/C$ were 1131.61 m^2/g, 0.78 cm^3/g and 2.77 nm, respectively, while the specific surface area of the spent 5 wt.% $Pd(OH)_2/C$ catalyst was 537.36 m^2/g, with an average pore volume of 0.50 cm^3/g and an average pore diameter of 3.72 nm. Comparing before and after the reaction, it can be clearly observed that the specific surface area of the reacted catalyst dropped sharply, and the average pore volume also dropped significantly. It shows that the pores inside the catalyst may be seriously blocked, and the great change in the physical structure properties of the catalyst carrier may be an important reason for the deactivation of the catalyst. However, the performance of the 5 wt.% Pd/C and 5 wt.% $Pd(OH)_2/C$ catalyst recovered to a certain extent after treatment with the mixture of chloroform and glacial acetic acid. As seen in Figure 6, the 5 wt.% Pd/C specific surface recovered to 1135.72 m^2/g and the 5% $Pd(OH)_2/C$ specific surface recovered to 706.9372 m^2/g indicating that this regeneration method helps remove organic substances, such as products covered on the surface of the catalyst after the reaction, and in releasing metal palladium active sites.

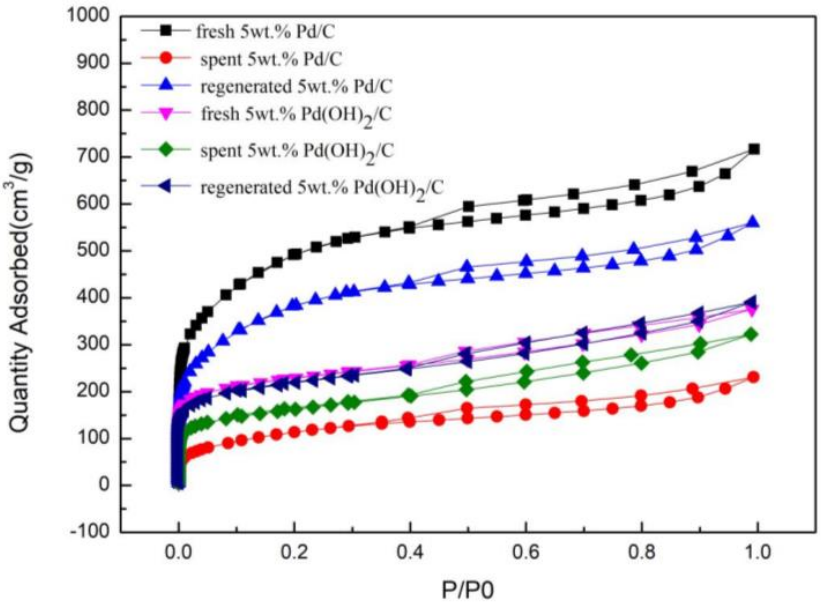

Figure 6. Nitrogen adsorption−desorption isotherms of fresh, spent and regenerated 5 wt.% Pd/C and 5 wt.% $Pd(OH)_2/C$ catalyst.

Table 4. Textural and structural properties of fresh, spent and regenerated 5 wt.% Pd/C and 5 wt.% $Pd(OH)_2/C$ catalyst.

Sample	Specific Area (m^2/g)	Pore Volume (cm^3/g)	Pore Size (nm)
Fresh 5 wt.% Pd/C	1493.7410	0.92	2.45
Spent 5 wt.% Pd/C	356.3837	0.29	3.31
Regenerated 5 wt.% Pd/C	1135.7178	0.72	2.44
Fresh 5 wt.% $Pd(OH)_2/C$	1131.61	0.78	2.77
spent 5 wt.% $Pd(OH)_2/C$	537.36	0.50	3.72
Regenerated 5 wt.% $Pd(OH)_2/C$	706.9372	0.61	3.43

The TG testing of 5 wt.% $Pd(OH)_2/C$ fresh, spent and regenerated catalyst with different treatments were performed in an N_2 atmosphere, as shown in Figure 7a with the fresh 5 wt.% $Pd(OH)_2/C$ treatment of glacial acetic acid for comparison. Figure 7b shows the spent 5 wt.% $Pd(OH)_2/C$ catalyst treated with glacial acetic acid. Figure 7c is the reacted 5 wt.% $Pd(OH)_2/C$ treated with the chloroform and glacial acetic acid mixture. The result of Figure 7a shows that there is a weight loss water peak at 70 °C, and an obvious weight loss peak near 200 °C, which may be the decomposition peak of the glacial acetic acid or the dehydration peak of $Pd(OH)_2$. The result in Figure 7b shows that the spent 5 wt.% $Pd(OH)_2/C$ catalyst has an obvious weight loss peak near 300 °C, indicating that there are a lot of blocking substances on the catalyst after the reaction. However, it is not possible to determine what this substance is, it could be a reactant, intermediate material or product. For the reactants of the reaction with a large molecular weight, the blockage of the pore will have a huge impact on the transmission of material, which directly leads to the yield of TADBIW. Compared with Figure 7b, its weight loss peak at 300 °C is much smaller in Figure 7c, and the mass loss rate is about 3%, which is greatly reduced when compared to the reacted catalyst which has a mass loss rate of about 15%. It shows that after the treatment, the blockage of the catalyst is greatly alleviated so that the mechanical reaction can still maintain a high activity.

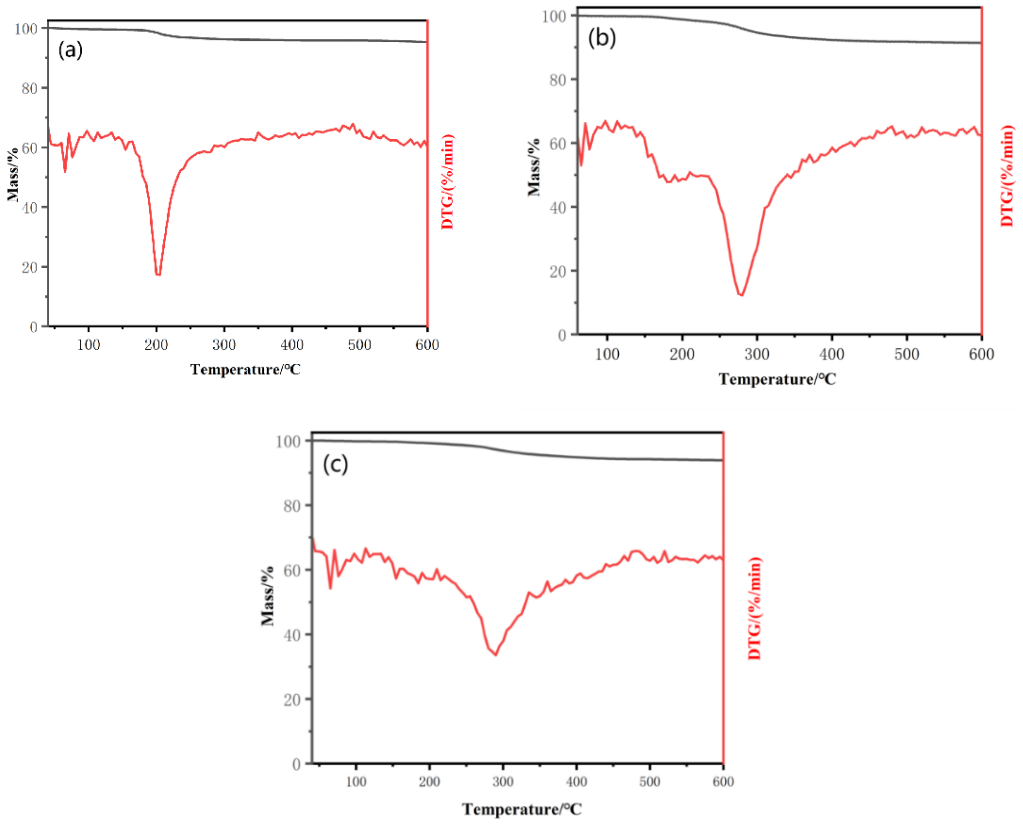

Figure 7. Thermogram of catalysts (**a**) fresh 5 wt.% $Pd(OH)_2/C$ catalyst treated with acetic acid; (**b**) 5 wt.% $Pd(OH)_2/C$ catalyst after reaction; and (**c**) 5 wt.% $Pd(OH)_2/C$ catalyst recovering with chloroform and glacial acetic acid.

3. Materials and Methods

3.1. Catalyst Preparation and Reaction Process

Pd catalysts with a loading of 5 wt.% were prepared using the deposition precipitation method. HBIW (5 g), DMF (50 mL), PhBr (0.1 mL), 0.5 g palladium supported as 5 wt.% $Pd(OH)_2/C$ (or 5 wt.% Pd/C) and Ac_2O (7 mL) were added to the micro. In the reactor, H_2

is passed three times to exhaust all the air in the reactor, and then H_2 is continuously fed to maintain the pressure of hydrogen at 0.4 MPa. The reaction was generally carried out for 12 h at temperatures below 40 °C.

3.2. Reaction Treatment and Yield Calculation

After the reaction, it was cooled to room temperature naturally, filtered and washed with absolute ethanol to obtain a mixture of product TADBIW and catalyst, and then placed in an oven for drying.The dry TADBIW and catalyst mixture was weighed, the mass denoted as W1, and the TADBIW was extracted from the mixture with Ac_2O. A white product (TADBIW, $C_{28}H_{32}N_6O_4$, mol. wt.: 516.60) was obtained and then measured by HPLC and 1H NMR (displayed in Figures S1 and S2, ESI) and the element analysis was as reported. The yield was calculated according to the weight of the white solids by subtracting that of the catalyst. Purity: 99.88%; 1H NMR (400 MHz, DMSO)δ: 7.56–7.30 (m, 10H), 6.71–6.21 (m, 2H), 5.57–5.20 (m, 4H), 4.18–3.93 (m, 4H), and 2.16–1.75 (m, 12H).

The yield was calculated using the following formula:

$$Y = \frac{n(TADBIW)}{n(HBIW)} = \frac{m(TADBIW)/M1}{m(HBIW)/M2} = \frac{(W1 - W2)/M1}{m(HBIW)/M2}$$

Among them, M_1 is the relative molecular mass (516.60 g/mol) of TADBIW, and M_2 is the relative molecular mass (708.95 g/mol) of HBIW.

3.3. Recovering Methods

Alkali washing method: first, dissolve the TADBIW solid in the mixed solid of catalyst and product with 50 mL of glacial acetic acid. The filtration and washing with absolute ethanol left the catalyst solid. The catalyst was then placed in an oven at 110 °C for 6 h and dried, then dissolved in 100 mL of 10 wt.% NaOH solution and stirred at 60 °C for 3 h. Finally, it was filtered and washed with absolute ethanol and deionized water in turn, placed in an oven for 12 h and then stored.

Hydrothermal treatment method: first, 50 mL of glacial acetic acid was used to dissolve the mixed solid of the catalyst and product. Filtration and washing with absolute ethanol left the catalyst solid. Then, the catalysts were dried for 6 h and then placed in a 250 mL hydrothermal kettle with 100 mL of DMF in a blast oven for 3 h, filtered and washed with absolute ethanol and dried in an oven for 12 h.

Roasting treatment: First, filtration and washing with absolute ethanol left the catalyst solid. The catalyst was then dried for 6 h, and then calcined in a tube furnace with N_2 as a protective atmosphere at a heating rate of 5 °C/min, from 40 °C to 250 °C (the other two groups were carried out at 300 °C and 500 °C, respectively), and maintained for 3 h.

The chloroform and glacial acetic acid mixture treatment: First, the catalyst and the product are treated with 20 mL of chloroform and 30 mL of glacial acetic acid into a uniform mixture at a temperature of 60 °C for 1 h. After filtration, the catalyst was dried for 6 h, then added to a mixture of 20 mL of chloroform and 30 mL of glacial acetic acid for 40 min, followed by sonication for 15 min, finally filtered, washed with absolute ethanol and deionized water, and then dried.

4. Conclusions

The causes of catalyst inactivation were explored using characterization techniques including AAS, XRD, TEM, BET, XPS and TG. The results showed that the main reason for catalyst deactivation was that a large amount of blockage accumulated in the pore of the catalyst after the reaction, which greatly weakened the transfer effect of the reactant HBIW. At the same time, the blockage may cover the precious metal palladium, making the reactant unable to contact the precious metal Pd. It directly blocks the catalytic reaction. Meanwhile, a regenerative treatment method for catalyst inactivation was developed, which used chloroform and glacial acetic acid as reagents, combined with stirring and ultrasonic operation to finally restore the catalyst activity. Moreover, the related pa-

rameters of the regenerated catalyst have little difference with those of the fresh catalyst, indicating that this treatment method can play a role in removing the blockage in the catalyst channel.

Supplementary Materials: The following supporting information can be downloaded at: https://www.mdpi.com/article/10.3390/catal12121547/s1, Figure S1: HPLC for the product from HBIW hydrogenolysis; Figure S2: ^{1}H NMR for the product from HBIW hydrogenolysis.

Author Contributions: Conceptualization, M.W. and J.Q.; methodology, M.W.; software, J.Q.; validation, S.L., J.J. and B.L.; formal analysis, M.W.; investigation, J.Q.; resources, B.L.; data curation, J.J.; writing—original draft preparation, M.W.; writing—review and editing, Q.Z., C.L., F.F. and J.L.; visualization, J.Q.; supervision, X.L.; project administration, Q.W.; funding acquisition, Q.Z. All authors have read and agreed to the published version of the manuscript.

Funding: This work was financially supported by the National Natural Science Foundation of China (22078292, 22008212, U20A20119, 21776258).

Conflicts of Interest: The authors declare no conflict of interest.

References

1. Cannizzo, L.F.; Edwards, W.W.; Wardle, R.B. Synthesis of 2,4,6,8,10,12-hexabenzyl-2,4,6,8,10,12-hexaazatetracyclo 5.5.0.05,9.03,11!dodecane. U.S. Patent 5723604A, 3 March 1998.
2. Tang, X.; Zhu, R.; Shi, T.; Wang, Y.; Niu, X.; Zhang, Y.; Zhu, J.; Li, W.; Hu, W.; Xu, R. Research progress and key issues of hydrodebenzylation of hexabenzylhexaazaisowurtzitane (HBIW) in the synthesis of high energy density material hexanitrohexaazaisowurtzitane (HNIW). *Materials* **2022**, *15*, 409. [CrossRef] [PubMed]
3. Viswanath, J.V.; Venugopal, K.J.; Rao, N.S.; Venkataraman, A. An overview on importance, synthetic strategies and studies of 2,4,6,8,10,12-hexanitro-2,4,6,8,10,12-hexaazaisowurtzitane (HNIW). *Def. Technol.* **2016**, *12*, 401–418. [CrossRef]
4. Norris, W.P.; Nielsen, A.T. Catalitic Synthesis of Caged Polynitraminepolynitramine. U.S. Patent 8017768A, 13 September 2011.
5. Lian, L.U.; Yu, O.U.; Li, C.I. Synthesis of HNIW from TADBIW. *J. Shijiazhuang Teach. Coll. June* **2003**.
6. Chapman, R.D.; Hollins, R.A. Processes for Preparing Certain Hexaazaisowurtzitanes and Their Use in Preparing Hexanitrohexaazaisowurtzitane. U.S. Patent 7875714B1, 25 July 2011.
7. Qiu, L.M.; Gong, X.D.; Zheng, J.; Xiao, H. Theoretical studies on polynitro-1,3-bishomopentaprismanes as potential high energy density compounds. *J. Hazard. Mater.* **2009**, *166*, 931–938. [CrossRef] [PubMed]
8. Duddu, R.; Dave, P.R. Process and Composition for Nitration of N-Nitric Acid at Elevated Temperatures to Form HNIW and Recovery of Grmma HNIW. U.S. Patent 6160113A, 12 December 2020.
9. Bayat, Y.; Hajimirsadeghi, S.S.; Pourmortazavi, S.M. Statistical optimization of reaction parameters for the synthesis of 2,4,6,8,10,12-hexanitro-2,4,6,8,10,12-hexaazaisowurtzitane. *Org. Process Res. Dev.* **2011**, *15*, 810–816. [CrossRef]
10. Bazaki, H.; Kawabe, S.; Miya, H. Synthesis and sensitivity of hexanitrohexaaza-isowurtzitane (HNIW). *Propellants Explos. Pyrotech.* **1998**, *23*, 333–336. [CrossRef]
11. Wardle, R.B.; Edwards, W.W. Improved Hydrogenolysis of 2,4,6,8,10,12-Hexabenzyl-2,4,6,8,10,12-Hexaazatetracyclo [5.5.0.05,9.03,11] Dodecane. W.O. Patent 9720785A1, 12 June 1997.
12. Nair, U.R.; Sivabalan, R.; Gore, G.M.; Geetha, M.; Asthana, S.N.; Singh, H. Hexanitrohexaazaisowurtzitane (CL-20) and CL-20-based formulations (review). *Combust. Explos. Shock Waves* **2005**, *41*, 121–132. [CrossRef]
13. Mandal, A.K.; Pant, C.S.; Kasar, S.M.; Soman, T. Process optimization for synthesis of CL-20. *J. Energetic Mater.* **2009**, *27*, 231–246. [CrossRef]
14. Simpson, R.L.; Lee, R.S.; Tillotson, T.M. Process for Preparing Energetic Materials. U.S. Patent 8075716B1, 13 December 2011.
15. Latypov, N.V.; Wellmar, U.; Goede, P. Synthesis and scale-up of 2,4,6,8,10,12-hexanitro-2,4,6,8,10,12-hexaazaisowurtzitane from 2,6,8,12-tetraacetyl-4,10-dibenzyl-2,4,6,8,10,12-hexaazaisowurtzitane (HNIW, CL-20). *Org. Process Res. Dev.* **2000**, *3*, 156–158. [CrossRef]
16. Renganathan, S.; Gore, G.M.; Nair, U.R.; Saikia, A.; Sikder, A.K.; Sethuramasharma, V. Process for Preparation of Tetraacetyl Hexaazaisowurtzitane (TAIW) and Its Nitration to Hexanitro-Hexaazaisowutzitane (CL-20). India Patent IN2007DE00577A, 26 September 2008.
17. Bayat, Y.; Mokhtari, J.; Farhadian, N.; Bayat, M. Heteropolyacids: An efficient catalyst for synthesis of CL-20. *J. Energetic Mater.* **2012**, *30*, 124–134. [CrossRef]
18. Wei, X.; Xu, J.; Li, H.; Long, X.; Zhang, C. Comparative study of experiments and calculations on the polymorphisms of 2,4,6,8,10,12-hexanitro-2,4,6,8,10,12-hexaazaisowurtzitane (CL-20) precipitated by solvent/antisolvent method. *J. Phys. Chem. C* **2016**, *120*, 5042–5051. [CrossRef]
19. Olah, G.A.; Squire, D.R. *Chemistry of Energetic Materials*; Academic Press: San Diego, CA, USA, 1991; pp. 95–123.
20. Chen, J.; Zheng, F.; Ou, Y. Study on the Kinetics of Hydrogenolysis Debenzylation of 2,4,6,8,10,12 Hexabenzyl 2,4,6,8,10,12 Hexaazaisowurtzitane(HBIW). *J. Beijing Inst. Technol.* **1999**.

21. Crampton, M.R.; Hamid, J.; Millar, R.; Ferguson, G. Studies of the synthesis, protonation and decomposition of 2,4,6,8,10,12-hexabenzyl-2,4,6,8,10,12-hexaazatetracyclo[5.5.0.0^{5,9}.0^{3,11}] dodecane (HBIW). *Jounal Chem. Soc.* **1993**, *5*, 923–929. [CrossRef]
22. Dong, K.; Sun, C.H.; Zhang, S.W.; Wang, H.Y.; Song, J.W.; Pang, S.P. Condensation mechanism of cage hexabenzyl-hexaazaisowurtzitane from glyoxal and benzylamine: A computational study. *New, J. Chem.* **2017**, *41*, 12694–12699. [CrossRef]
23. Malekzadeh, A.M.; Shokrollahi, S.; Ramazani, A.; Rezaei, S.J.; Asiabi, P.A.; Joo, S.W. Synthesis of hexabenzyl-hexaazaisowurtzitane (HBIW) under ultrasound irradiation with Fe_3O_4@PCA nanoparticles as an efficient and reusable nanomagnetic catalyst. *Cent. Eur. J. Energetic Mater.* **2017**, *14*, 336–350. [CrossRef]
24. Maksimowski, P.; Goofit, T.; Tomaszewski, W. Palladium Catalyst in the HBIW Hydrodebenzylation Reaction. Deactivation and Spent Catalyst Regeneration Procedure. *Cent. Eur. J. Energetic Mater.* **2016**, *13*, 333–348. [CrossRef]
25. Bellamy, A. Reductive debenzylation of hexabenzylhexaazaisowurtzitane. *Tetrahedron* **1995**, *51*, 4711–4722. [CrossRef]
26. Nielsen, A.T. Caged Polynitramine Compound. U.S. Patent 5693794A, 2 December 1997.
27. Nielsen, A.T.; Nissan, R.A.; Vanderah, D. Polyazapolycyclics by condensation of aldehydes with amines. 2. formation of 2,4,6,8,10,12-hexabenzyl-2,4,6,8,10,12-hexaazatetra-cyclo[5.5.0.0$^{5.9}$.0^{3,11}] dodecanes from glyoxal and benzylamines^{1,2}. *J. Org. Chem.* **1990**, *55*, 1459–1466. [CrossRef]
28. Dong, K.; Sun, C.H.; Song, J.W.; Wei, G.X.; Pang, S.P. Synthesis of 2,6,8,12-Tetraacetyl-2,4,6,8,10,12-hexaazaisowurtzitane (TAIW) from 2,6,8,12-Tetraacetyl-4,10-dibenzyl-2,4,6,8,10,12-hexaazaisowurtzitane (TADBIW) by Catalytic Hydrogenolysis Using a Continuous Flow Process. *Org. Process Res. Dev.* **2014**, *18*, 1321–1325. [CrossRef]
29. Lou, D.; Wang, H.; Liu, S.; Li, L.; Zhao, W.; Chen, X.; Wang, J.; Li, X.; Wu, P.; Yang, J. PdFe bimetallic catalysts for debenzylation of hexabenzylhexaazaisowurtzitane (HBIW) and tetraacetyldibenzylhexaazaisowurtzitane (TADBIW). *Catal. Commun.* **2018**, *109*, 28–32. [CrossRef]
30. Dong, K.; Chen, Y.; Zhang, Y.Y. The highly effective hydrogenolysis-based debenzylation of tetraacetyl-dibenzyl-hexaazaisowurt zitane(TADBIW) using a palladium/DOWEX catalyst having a synergistic effect. *J. Energetic Mater.* **2017**, *35*, 421–429. [CrossRef]
31. Bayat, Y.; Malmir, S.; Hajighasemali, F. Reductive debenzylation of hexabenzyl-hexaazaisowurtzitane using multi-walled carbon nanotube-supported palladium catalysts: An optimization approach. *Cent. Eur. J. Energetic Mater.* **2015**, *12*, 439–458.
32. Chen, S.; Liu, S.; Men, Y.; Li, L.; Li, X.; Pan, X.; Sun, C.; Xiong, L.; Niu, X.; An, W.; et al. Synergistic Catalysis of PdFe Bimetallic Nanoparticles Supported on SiO_2 for Hydrogenative Cleavage of C–N Bonds. *ACS Appl. Nano Mater.* **2021**, *4*, 6020–6029. [CrossRef]
33. Studer, M.; Blaser, H.U. Influence of catalyst type, solvent, acid and base on the selectivity and rate in the catalytic debenzylation of 4-chloro-N,N-dibenzyl aniline with Pd/C and H_2. *J. Mol. Catal. A Chem.* **1996**, *112*, 437–445. [CrossRef]
34. Zhang, M.; Liu, S.; Li, L.; Li, X.; Huang, H.; Yin, J.; Shao, X.; Yang, J. Effect of carbon supports on Pd catalyst for hydrogenation debenzylation of hexabenzylhexaazaisowurtzitane (HBIW). *J. Energetic Mater.* **2016**, *35*, 251–264. [CrossRef]
35. Liu, W.; Li, S.; She, C.; Yang, Y.; Chen, S.; Jin, S.; Chen, K. Excellent stability of Pd/mpg-C_3N_4 in catalytic hydrodebenzylation of 2,4,6,8,10,12-Hexabenzyl-2,4,6,8,10,12-hexaazaisowurtzitane (HBIW). *Appl. Catal. A Gen.* **2021**, *624*, 118310–118318. [CrossRef]
36. Zhao, W.; Liu, S.; Wang, H.; Yang, J.; Chen, X. Ultrasmall Pd Nanoparticles Supported on TiO_2 for Catalytic Debenzylation via Hydrogenative C–N Bond Cleavage. *ACS Appl. Nano Mater.* **2020**, *4*, 159–166. [CrossRef]
37. Liu, S.; Ji, F.; Li, X.; Pan, X.; Chen, S.; Wang, X.; Zhang, Y.; Men, Y. Stick-like mesoporous titania loaded Pd as highly active and cost effective catalysts for hydrodebenzylation of hexabenzylhexaazaisowurtzitane (HBIW). *Mol. Catal.* **2019**, *477*, 110556. [CrossRef]
38. Bayat, Y.; Ebrahimi, H.; Fotouhi-Far, F. Optimization of Reductive Debenzylation of Hexabenzylhexaazaisowurtzitane (the Key Step for Synthesis of HNIW) Using Response Surface Methodology. *Org. Process Res. Dev.* **2016**, *16*, 1733–1738. [CrossRef]
39. Koskin, A.P.; Simakova, I.L.; Parmon, V.N. Reductive debenzylation of hexabenzyl-hexaazaisowurtzitane—The key step of the synthesis of polycyclic nitramine hexanitrohexaazaisowurtzitane. *Russ. Chem. Bull.* **2007**, *56*, 2370–2375. [CrossRef]
40. Maksimowski, P.; Fabijańska, A.; Adamiak, J. Tetraacetyl-dibenzyl-hexaazaisowurtzitane nitrosation-studies on scale-up synthesis of HNIW. *Propellants Explos. Pyrotech.* **2010**, *35*, 353–358. [CrossRef]
41. Fotouhi-Far, F.; Bashiri, H.; Hamadanian, M. Study of Deactivation of Pd$(OH)_2$/C Catalyst in Reductive Debenzylation of Hexabenzylhexaazaisowurtzitane. *Propellants Explos. Pyrotech.* **2017**, *42*, 213–219. [CrossRef]